Biochemical and Biophysical Research Communications 503 (2018) 822–829

Contents lists available at ScienceDirect

Biochemical and Biophysical Research Communications

journal homepage: www.elsevier.com/locate/ybbrc

Comparative folding analyses of unknotted versus trefoil-knotted ornithine transcarbamylases suggest stabilizing effects of protein knots

Manoj Kumar Sriramoju [a], Tzu-Jing Yang [a, b], Shang-Te Danny Hsu [a, b, *]

[a] Institute of Biological Chemistry, Academia Sinica, Taipei, 11529, Taiwan
[b] Institute of Biochemical Sciences, National Taiwan University, Taipei, 10617, Taiwan

ARTICLE INFO

Article history:
Received 11 June 2018
Accepted 15 June 2018
Available online 21 June 2018

Keywords:
Knotted protein
Protein folding
SAXS
HDX-MS
Ornithine transcarbamylase

ABSTRACT

Ornithine transcarbamylases (OTCs) are conserved enzymes involved in arginine biosynthesis in microbes and the urea cycle in mammals. Recent bioinformatics analyses identified two unique OTC variants, N-succinyl-L-ornithine transcarbamylase from *Bacteroides fragilis* (*Bf*SOTC) and N-acetyl-L-ornithine transcarbamylase from *Xanthomonas campestris* (*Xc*AOTC). These two variants diverged from other OTCs during evolution despite sharing the common tertiary and quaternary structures, with the exception that the substrate recognition motifs are topologically knotted. The OTC family therefore offers a unique opportunity for investigating the importance of protein knots in biological functions and folding stabilities. Using hydrogen-deuterium exchange-coupled mass spectrometry, we compared the native dynamics of *Bf*SOTC and *Xc*AOTC with respect to the unknotted ornithine transcarbamylase from *Escherichia coli* (*Ec*OTC). Our results suggest that, in addition to substrate specificity, the knotted structures in *Xc*AOTC and *Bf*SOTC may play an important role in stabilizing the folding dynamics, particularly around the knotted structural elements.

© 2018 Elsevier Inc. All rights reserved.

1. Introduction

Knotted proteins entwine themselves in their backbone to form a knot that makes them topologically constrained [1–3]. The first example of a knotted protein, carbonic anhydrase, was described in 1977 by Richardson [4] and it was later characterized more systematically and mathematically in 1994 by Mansfield [5]. Since then, more than 1000 knotted protein structures have been identified in the protein data bank [6]. These knotted proteins were classified according to their topologies, which include trefoil knots, figure-eight knots, Gordian knots, and Stevedore's knot [2,7].

Several knotted motifs are conserved throughout evolution, some are located near the catalytic sites and these evolutionary conservations suggest functional roles of protein knots [8,9]. Recent studies have demonstrated that knotted proteins exhibit mechanostabilities against vectorial unfolding [10,11]. Nonetheless, there are few examples of protein families that have both knotted and unknotted protein members to allow pair-wise comparisons to ascribe functional attributions of protein knots. In this regard, *Xc*AOTC and *Bf*SOTC are unique, evolutionarily divergent, and contain trefoil knotted structures while the rest of the OTC family members are unknotted (Fig. 1 and Supplementary Fig. S1) [12,13].

Here we chose three members within the OTC superfamily that belong to the OTCace_N clan [14], namely the unknotted *Ec*OTC, the knotted *Bf*SOTC, and the knotted *Xc*AOTC to carry out comparative analyses of their folding dynamics in the context of topological knots. These proteins are homotrimeric and the individual protomers share a high degree of structural similarity with the exception of the knot-promoting motifs, however they share limited sequence similarity (Fig. 1). The individual monomer possesses a carbamyl phosphate (CP) binding domain and a substrate-binding (SSB) domain. The CP domains of these proteins are structurally similar whereas the SSB domain in the unknotted *Ec*OTC protein is distinct from those of *Bf*SOTC and *Xc*AOTC in the knot core region. The entanglement of the 240s region of *Bf*SOTC and *Xc*AOTC proteins with the proline-rich (Pro) region results in the formation of knot [15,16], while the 240s region hangs over the Pro region in *Ec*OTC to make it unknotted [12,13,17]. According to KnotProt [6], *Bf*SOTC and *Xc*AOTC are two of the most deeply knotted proteins in

* Corresponding author. Institute of Biological Chemistry, Academia Sinica 128, Section 2, Academia Road, 11529, Taipei, Taiwan.
E-mail address: sthsu@gate.sinica.edu.tw (S.-T.D. Hsu).

https://doi.org/10.1016/j.bbrc.2018.06.082
0006-291X/© 2018 Elsevier Inc. All rights reserved.

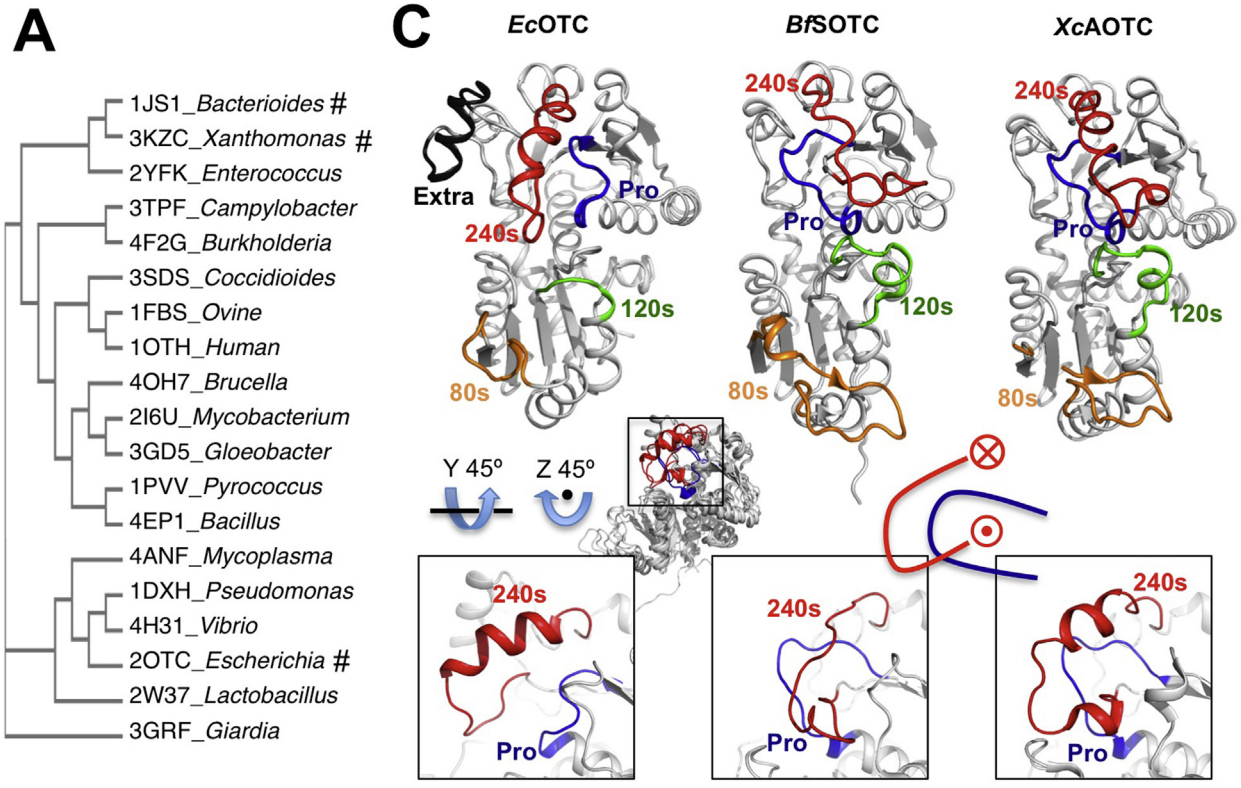
A
1JS1_Bacterioides #
3KZC_Xanthomonas #
2YFK_Enterococcus
3TPF_Campylobacter
4F2G_Burkholderia
3SDS_Coccidioides
1FBS_Ovine
1OTH_Human
4OH7_Brucella
2I6U_Mycobacterium
3GD5_Gloeobacter
1PVV_Pyrococcus
4EP1_Bacillus
4ANF_Mycoplasma
1DXH_Pseudomonas
4H31_Vibrio
2OTC_Escherichia #
2W37_Lactobacillus
3GRF_Giardia
C
EcOTC
BfSOTC
XcAOTC
Extra
Pro
240s
120s
80s
Y 45°
Z 45°

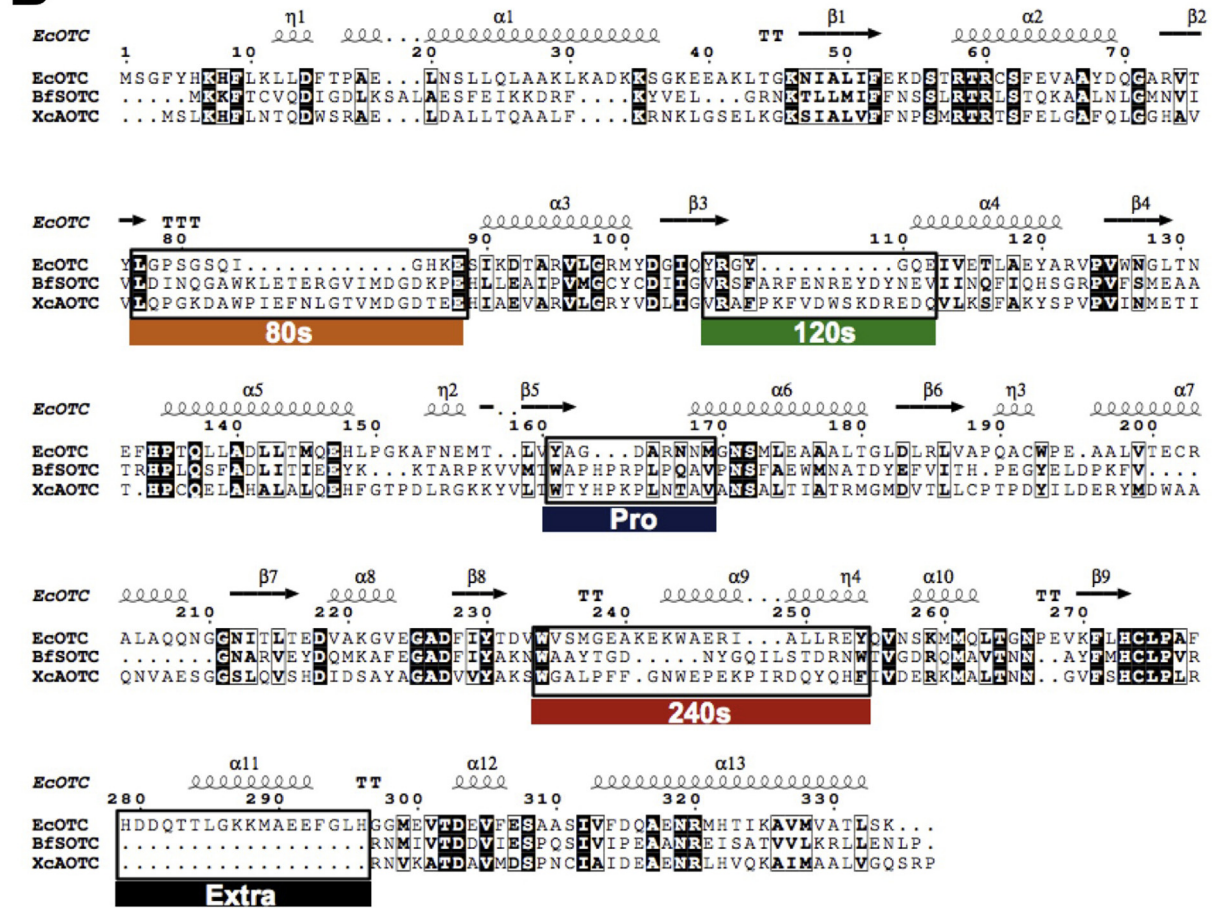
B
EcOTC
BfSOTC
XcAOTC
80s
120s
Pro
240s
Extra

the database, with more than 170 and 80 flanking residues in the N- and C-terminal ends, respectively, and a knot core of more than 60 residues long (Fig. 1, Supplementary Fig. S2, and Supplementary Table S1). As a comparison, the most studied trefoil knotted YibK and YbeA are considered deeply knotted while the threading C-terminal helices are about 40 residues in length. Functionally, the knot core region of the knotted OTCs and the corresponding region in unknotted OTC are involved in substrate binding. Earlier biochemical studies on these OTC variants established their distinct substrate specificities (Supplementary Fig. S3) [16,18,19]. However, little is known about the contributions of topological knots in terms of their folding stabilities. Here we compare their native folding dynamics by hydrogen-deuterium exchange coupled mass spectrometry (HDX-MS). Our findings suggested a stabilizing effect in the knotted proteins compared to the unknotted proteins manifested by reduced internal dynamics in the loop regions that are involved in knot formation.

2. Material and methods

2.1. Plasmid construction, recombinant protein expression and purification

Codon-optimized synthetic genes corresponding to the open reading frames of *Ec*OTC, *Bf*SOTC, and *Xc*AOTC were obtained from GeneScript, USA. These DNA sequences were sub-cloned into a pET-z2 vector, a kind gift from Dr. Arie Geerlof (Helmholtz Center, Munich, Germany), resulting in a fusion protein with the N-terminal His-tag by a Z2 fusion tag that is cleavable by TEV protease. The plasmids were individually transformed into the BL21 (DE3) *E. coli* strain and purified using previously reported protocols [20,21]. The protein purity was verified by SDS-PAGE. Because the crystal structure of *Ec*OTC was determined at pH 7.5 [22], while those of *Bf*SOTC and *Xc*AOTC were determined in Tris buffer at pH 8.0 [15,23], we therefore chose to perform the experiments in Tris buffer pH 8.0 unless otherwise stated.

2.2. SAXS

Size exclusion chromatography-coupled small angle X-ray scattering (SEC-SAXS) experiments were carried on the beamline BL23A at the National Synchrotron Radiation Research Center (NSRRC, Hsinchu, Taiwan). All SAXS data were processed and analyzed using the previously reported protocol [24].

2.3. GdnHCl-induced unfolding monitored by intrinsic fluorescence and far-UV CD spectroscopy

*Ec*OTC, *Bf*SOTC, and *Xc*AOTC were incubated in different GdnHCl concentrations between 0 and 2.5 M. The protein and buffer were mixed in a 1:9 ratio to a final concentration of 2 μM. The samples were incubated at 25 °C, and the data were collected at 16, 40, 64, and 136 h post-GdnHCl incubation. The intrinsic fluorescence of the protein samples was monitored by exciting the samples at 280 nm and recording the emission from 300 to 500 nm with an interval of 2 nm. The data were collected at 25 °C in Infinite M1000PRO plate reader (TECAN, Switzerland). The data were subjected to SVD analysis as described previously [20,21]. For far-UV CD spectra, identical conditions were used with 5 μM protein concentration. The spectra were monitored between 210 and 260 nm with an interval of 1 nm using a 1 mm path-length cuvette (Helma, Germany) and the Jasco 815 CD spectrometer (Jasco, Japan). The CD signals at 222 nm were plotted as a function of GdnHCl concentration. All data were fit to a two-state folding model to determine the $[D]_{50\%}$ values.

2.4. HDX-MS analysis

HDX-MS measurements were carried out in a fully automated mode using the SYNAPT G2-Si HDMS system equipped with a LEAP robotic liquid handler (Waters Cooperation). The data collection was carried out by 20-fold dilution of the protein samples (80 μM) with deuterated buffer (5 mM potassium phosphate, adjusted to a pD value of 7.0, corresponding to a pH meter reading of 6.6 due to isotope effect) to trigger HDX for 0, 0.5, 10, 30, 60, 120, and 240 min at 25 °C (in triplicates), followed by an 1:1 mixing with the quenching buffer (50 mM potassium phosphate, pH 2.3 in H_2O) at 0 °C, online-digestion using an immobilized pepsin digestion column (Waters Enzymate BEH Pepsin, 2.1 × 30 mm), trapping using a C18 trapping column (Acquity BEH VanGuard 1.7 μm, 2.1 × 5.0 mm), and separating the peptides by a linear acetonitrile-gradient (5–40% of solution B consisting of 0.2% formic acid, 100% acetonitrile, pH 2.5, at a flow rate of 40 μL/min in 7 min, the blending solution A, consisting of 0.2% formic acid, pH 2.5 in H_2O) through a C18 analytic column (Acquity BEH C18: 1.7 μm, 1.0 × 100 mm). All columns were temperature-controlled at 4 °C to minimize back-exchange.

The data were processed by ProteinLynx Global Server (PLGS, Waters Cooperation) to identify the individual peptides and subsequently processed by DynamX (Waters Cooperation) using parameters: minimum intensity of 1000; minimum product ions per amino acid of 0.3; maximum MH^+ error of 5 ppm; and file threshold of three. A reference molecule [(Glu^1)-fibrinopeptide B human (CAS No 103213-49-6, Merck)] was used to lock mass with an expected molecular weight of 785.8426 Da. Only peptides that were commonly found in all triplicated experiments were considered for HDX-MS analyses. The fractional deuterium uptakes of individual peptides were extracted by DynamX to generate heat-maps as a function of residue number, and to facilitate structural mapping onto the crystal structures using PyMOL (Schrödinger, U.S.A.).

3. Results

3.1. SAXS confirmed the homotrimer quaternary structures of the OTCs

OTCs are key enzymes involved in the metabolism of arginine biosynthesis in bacteria and plants, and the urea cycle in mammals [25,26]. A large number of crystal structures of OTC variants have been reported, and they can form either dodecamers or homotrimers. In the case of *Ec*OTC, *Bf*SOTC, and *Xc*AOTC, the most likely

Fig. 1. Evolutionary and structural comparison of OTC variants. A. Phylogenetic tree representing the OTCs from different species (figure generated by Clustal Omega, https://www.ebi.ac.uk/Tools/msa/clustalo). Octothorpes indicate the three proteins studied herein. B. Sequence alignment of the unknotted *Ec*OTC, and the knotted *Bf*SOTC and *Xc*AOTC. The structural alignment was made by ESPript 3.0 (http://espript.ibcp.fr/ESPript/ESPript) using the crystal structure of *Ec*OTC (PDB ID: 2OTC) as input. C. Cartoon representations of monomeric crystal structures of *Ec*OTC, *Bf*SOTC, and *Xc*AOTC aligned in the same orientation. The unique structural motifs are colored and labeled as defined in B. The three structures are superimposed and rotated around the Y- and Z-axes by 45° as indicated below to highlight the loop threading (shown in blue and red for the Pro and 240s, respectively) in the knotted *Bf*SOTC and *Xc*AOTC in comparison to the non-threading loops in *Ec*OTC: the expanded views are shown below. The inset on the right hand side illustrate the loop threading by showing the Pro loop (shown in blue) in-plane and the threading 240s loop (shown in red) pointing out of the plane from within the Pro loop and loops back into the plane from above. (For interpretation of the references to color in this figure legend, the reader is referred to the Web version of this article.)

quaternary structures based on their crystal contacts are homotrimers. To evaluate their oligomeric states in the solution state, we employed SAXS to rapidly determine their structures and assembly under the same experimental conditions that were used for subsequent biophysical and biochemical analyses [21,27]. SEC-SAXS ensured that the samples were monodispersed in terms of their oligomeric states and the resulting SAXS profiles of recombinant *Ec*OTC, *Bf*SOTC, and *Xc*AOTC indicated compactly folded structures with well-defined bell shape distributions in the Kratky plots (Fig. 2). Guinier plot analyses yielded the radii of gyration (R_g) of 31.41 ± 0.08, 31.72 ± 0.06, and 31.17 ± 0.07 Å for *Ec*OTC, *Bf*SOTC, and *Xc*AOTC, respectively. These values are consistent with the theoretical values calculated from the crystal structures as well as with the R_g values derived from real space pair-wise distance distributions (Table 1). At a quaternary structure level, the domain architectures observed in the solution state were consistent with the reported crystal structures (Fig. 2).

Table 1
SAXS parameters of the OTCs.

Protein	Radius of gyration (Å)		PDB entry	D_{max} (Å)
	SAXS Guinier fit	Crystal structure		
*Ec*OTC	31.41 ± 0.08	30.7	2OTC	97.8
*Bf*SOTC	31.72 ± 0.06	30.8	1JS1	100.2
*Xc*AOTC	31.17 ± 0.07	30.8	3KZC	98.4

3.2. Knotted BfSOTC and XcAOTC require higher amount of chemical denaturant to unfold than does unknotted EcOTC

We next carried out chemical denaturation of OTC variants by monitoring the intrinsic fluorescence. We monitored changes in the intrinsic fluorescence as a function of guanidine hydrochloride (GdnHCl) concentration. The titration series were subject to singular value decomposition (SVD) analysis to identify the number of transitions associated with the GdnHCl-induced unfolding [20,28]. For all three OTCs, only one apparent transition was observed (Supplementary Fig. S4), we therefore used the simplest two-state unfolding model assuming a native (N) homotrimer to a denatured (D) monomer (N_3-3D) scenario to determine the transition points, *i.e.*, $[D]_{50\%}$ values. By incubating the samples over a period of one week and taking fluorescence data at various time points (16, 40, 64 and 136 h), the $[D]_{50\%}$ values continuously drifted towards lower GdnHCl concentrations, indicating very slow unfolding kinetics for all three OTC variants (Fig. 3), Given that all OTC variants are homotrimeric in solution, we examined whether their unfolding processes are protein concentration-dependent. We repeated the time-dependent GdnHCl-induced unfolding analyses of the OTCs

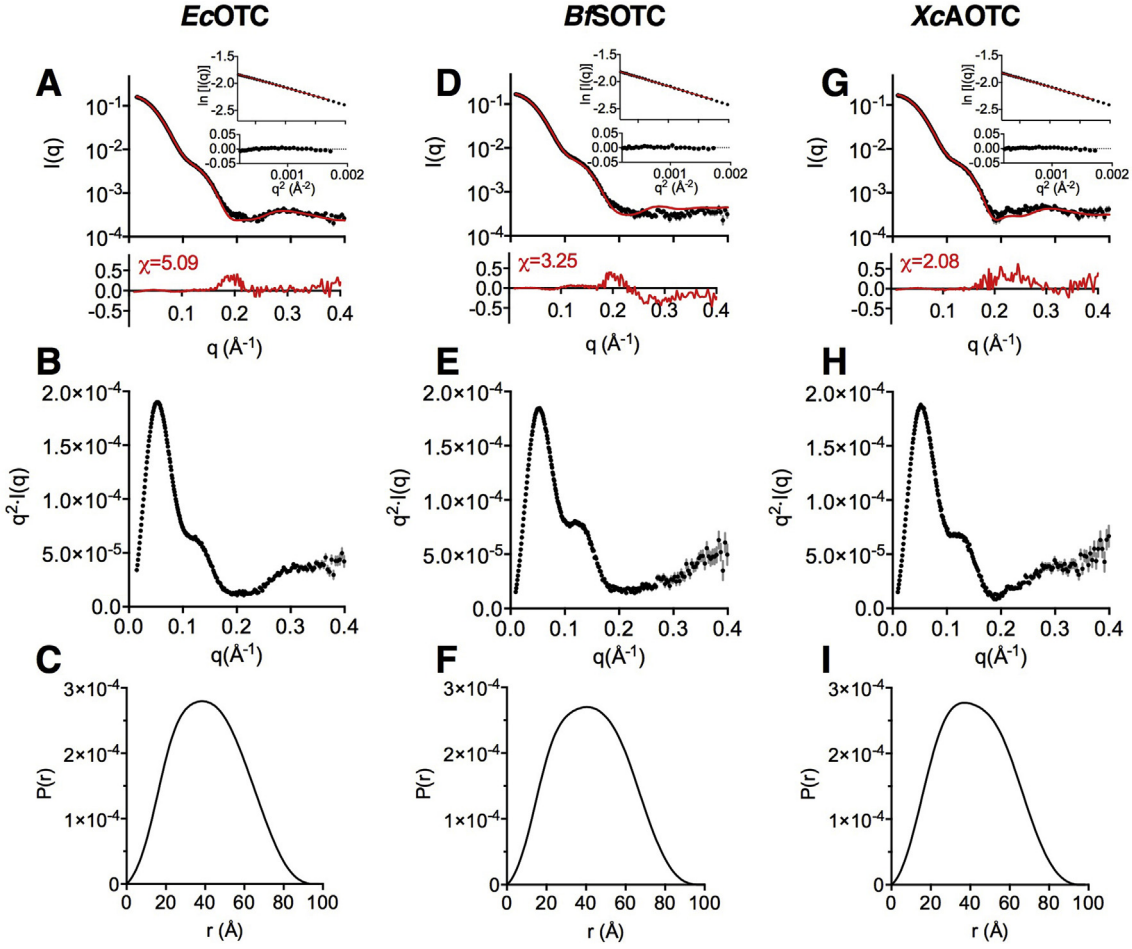

Fig. 2. SAXS analysis of *Ec*OTC, *Bf*SOTC, and *Xc*AOTC. Comparison of the experimental (black) and back-calculated SAXS profiles based on the crystal structures (red) of *Ec*OTC (A), *Bf*SOTC (D), and *Xc*AOTC (G). The fitting residues shown below in red with the associated χ-values indicated. Guinier plots and fitting residues are shown as insets. Kratky plots of *Ec*OTC (B), *Bf*SOTC (E), and *Xc*AOTC (H); pair-wise distance distribution, P(r), of *Ec*OTC (C), *Bf*SOTC (F), and *Xc*AOTC (I). (For interpretation of the references to color in this figure legend, the reader is referred to the Web version of this article.)

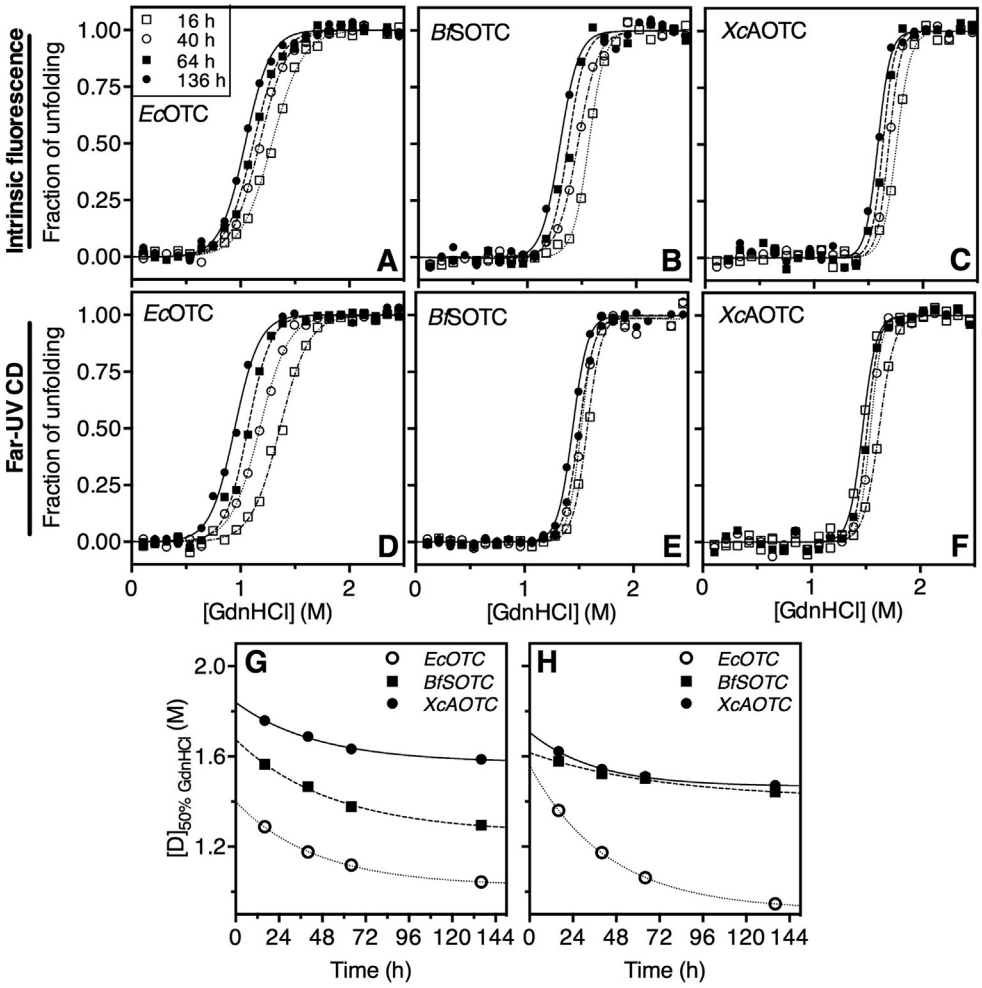

Fig. 3. GdnHCl-induced unfolding of OTC variants monitored by intrinsic fluorescence and far-UV CD spectroscopy. Fractional unfolded populations of *Ec*OTC, *Bf*SOTC, and *Xc*AOTC derived from SVD analyses of intrinsic fluorescence (A, B, C) and CD signals at 222 nm (D, E, F). The transition points $[D]_{50\%}$ as a function of incubation time were fit to a single exponential decay function for intrinsic fluorescence (G) and far-UV CD spectroscopy (H).

with different protein concentrations ranging between 0.2 and 10 μM (Supplementary Fig. S5). In all cases, only a single transition was observed in the unfolding curve (Fig. 3 and Table 2).

To cross-validate the intrinsic fluorescence data, we repeated the same GdnHCl-induced unfolding analyses under identical conditions, using far-UV CD spectroscopy. The far-UV CD spectra of all three OTCs showed clear loss of signals on increasing GdnHCl concentration, and plateaued after passing the transition points that resembled random coil-like spectral appearances (Fig. 3 and Supplementary Fig. S4). We obtained similar $[D]_{50\%}$ values at 16, 40, 64 and 136 h after incubation with GdnHCl and compared the results with those derived from the intrinsic fluorescence measurements (Table 2). The results suggested that both intrinsic fluorescence and far-UV CD reported on similar global unfolding events: knotted proteins *Bf*SOTC and *Xc*AOTC required higher amount of chemical denaturant to unfold than the unknotted *Ec*OTC.

Table 2
Plateau transition GdnHCl concentrations $[D]_{50\%}$ of OTC variants derived from intrinsic fluorescence and far-UV CD data.

Protein	$[D]_{50\%}$ (M)	
	Intrinsic Fluorescence	Far-UV CD
*Ec*OTC	1.02 ± 0.01	0.92 ± 0.01
*Bf*SOTC	1.26 ± 0.02	1.41 ± 0.03
*Xc*AOTC	1.57 ± 0.01	1.47 ± 0.01

3.3. Internal dynamics of OTC revealed by HDX-MS analysis

In addition to analyzing the folding stabilities of the OTC variants, we applied hydrogen-deuterium exchange mass spectroscopy (HDX-MS) to characterize the internal dynamics in these proteins [29]. In total, 145, 174 and 105 common peptides were identified from triplicated datasets of 21 independent HDX-MS injections for *Ec*OTC, *Bf*SOTC and *Xc*AOTC, corresponding to a sequence coverage of 95.5, 92.5 and 88.5%, respectively (Supplementary Figs. S6–S12 and Supplementary Table S3). The overall relative fractional deuterium uptake was less than 50%, even for the solvent-exposed loop regions. The typical standard deviations of the absolute deuterium uptake values derived from the triplicate experiments were less than 0.2 Da per peptide at each time point (Supplementary Table S4). Structural mapping of the fractional uptakes onto the monomeric structures of OTCs indicated that *Ec*OTC collectively exhibited higher deuterium uptakes compared to those of *Bf*SOTC and *Xc*AOTC (Fig. 4). The results showed relative lower deuterium uptakes at the trimer interfaces of all OTC variants, which may be sequestered from solvent exposure.

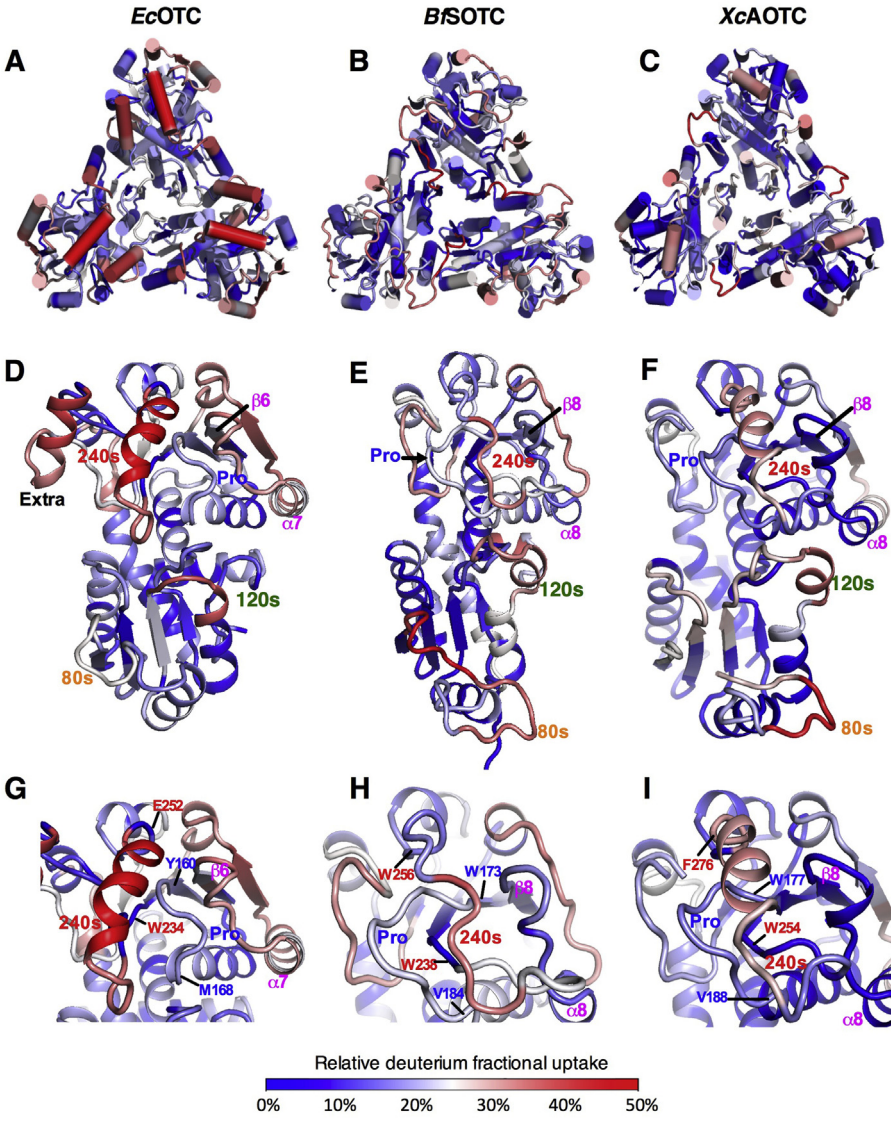

Fig. 4. HDX-MS analyses of the OTC variants. Structural mapping of relative deuterium uptake levels on *Ec*OTC (A, D, G), *Bf*SOTC (B, E, H) and *Xc*AOTC (C, F, I). The cartoon representations are color ramped from blue to white to red, corresponding to 0–50% fractional deuterium uptake after 4 h of HDX, as indicated by the scale bar shown below. Top panels (A, B, C): the homotrimeric structures of OTC variants; middle panels (D, E, F): cartoon representations of single chains of the trimers; bottom panels (G, H, I): enlarged view of the knotted core region of *Bf*SOTC (H) and *Xc*AOTC (I) and the corresponding region in unknotted *Ec*OTC (G). The Pro regions of *Ec*OTC (Y160-M168), *Bf*SOTC (W173-V184), and *Xc*AOTC (W177-V188) and the 240s regions of *Ec*OTC (W234-E252), *Bf*SOTC (W238-W256), and *Xc*AOTC (W254-F276) are labeled accordingly. (For interpretation of the references to color in this figure legend, the reader is referred to the Web version of this article.)

Detailed examinations of the monomeric structures revealed that the most pronounced deuterium uptake took place in the 240s and Extra regions of *Ec*OTC. In the case of the Extra region of *Ec*OTC, more than 30% relative deuterium uptake was observed**.** The 80s and 120s regions that are present in the knotted *Bf*SOTC and *Xc*AOTC, but not in the unknotted *Ec*OTC, showed more than 30% of relative deuterium uptake suggesting the internal flexibility in knotted proteins. In contrast to the 80s and 120s regions, the Pro region, which is part of the knotted structural motif, showed relatively lower deuterium uptake of about 15% (Fig. 4). The 240s region in *Ec*OTC showed relatively high flexibility compared to that of *Bf*SOTC and *Xc*AOTC. Interestingly, the region between β6 and α7 (P189-L198) of *Ec*OTC exhibited enhanced flexibility, while the corresponding regions in *Bf*SOTC (β8 and α8; F199-D210) and *Xc*AOTC (β8 and α8; L206-D215) showed significant protection from solvent exposure with limited deuterium uptake (<5%). Collectively, the HDX-MS results indicated that the unknotted *Ec*OTC exhibits more abundant internal dynamics compared to the knotted *Bf*SOTC and *Xc*AOTC proteins. The knot forming loop regions (Pro and 240s) are more protected from solvent exchange in knotted proteins than the unknotted ones, suggesting that the knotted elements can indeed reduce the internal dynamics and stabilize the knotted proteins.

The fractional deuterium uptakes reflect the local fluctuations (internal dynamics) on the minute to hour timescale. We compared the HDX-MS-derived dynamics information with the crystallographic B-factors, which correspond to the variance of the isotropic distributions of individual atoms observed in the crystal structures. The experimental B-factors can be compared with root-mean-squared fluctuations of individual atoms observed in molecular dynamics simulations [30]. While there existed qualitative correlations between the HDX-MS- and experimental B-factor-derived local fluctuations according to visual inspection of the structural mapping of the fractional deuterium uptake and the

crystallography B-factors (loop regions that exhibited high deuterium uptakes also showed high B-factors; Supplementary Fig. S13), quantitative correlations between the two experimental variables were limited with the correlation coefficients (R^2) ranging between 0.12 and 0.36. The correlations between the knotted *Bf*SOTC and *Xc*AOTC were slightly better than that of the unknotted *Ec*OTC.

4. Discussion

Experimental annotations of the potential functional importance of protein knots are challenging because of the lack of good reference points. It is not trivial to introduce or remove knotted structure elements by protein engineering to enable comparative analyses with the same baseline contributions from the sequence and structure variations. It has indeed been demonstrated by Yeates and colleagues that by concatenating a homodimeric protein HP0242, it is possible to generate a trefoil-knotted protein without perturbing its three-dimensional structure. The results elegantly illustrated that knotting increases folding stability and reduces the intrinsic unfolding rate [31,32]. Nevertheless, no natural occurring pairs of knotted versus unknotted homologs have been experimentally characterized to evaluate the contributions of protein knots to the folding stabilities. In this context, the OTC family is uniquely suited for such comparative analyses because of the naturally occurring examples of the knotted and unknotted forms that share similar overall tertiary and quaternary structures, such as the targets that were selected for the present study, namely unknotted *Ec*OTC versus knotted *Bf*SOTC and *Xc*AOTC (Fig. 1).

In this study, we evaluated the folding of *Ec*OTC, *Bf*SOTC, and *Xc*AOTC by chemical denaturation as well as their internal dynamics under native conditions by HDX-MS. We first employed SEC-SAXS to establish that all OTCs form stable homotrimers in solution with comparable quaternary structures (Fig. 2). During the intrinsic fluorescence-based unfolding analyses, we noticed the markedly slower unfolding behaviors of all three OTC variants: They took more than 136 h to reach plateau values (Fig. 3). Similar results were obtained by repeating the same unfolding analyses monitored by far-UV CD spectroscopy. In light of the folding stabilities derived from chemical unfolding experiments, we performed HDX-MS analyses under native conditions to evaluate the local folding dynamics by examining the deuterium uptakes of the individual peptide fragments as a function of HDX time. Without the need to trigger unfolding events by an elevated temperature or concentrated chemical denaturants, HDX-MS provides native state dynamics information that can be mapped onto different structural motifs within the three-dimensional structures.

In line with the GdnHCl-based unfolding analyses (Fig. 3), *Ec*OTC exhibits the most abundant structural fluctuations within the homotrimeric assembly compared to *Bf*SOTC and *Xc*AOTC (Fig. 4). A closer examination into the structural features of HDX-MS patterns revealed that the most abundant HDX process in *Ec*OTC corresponded to the unknotted 240s and Pro regions whereas the intertwined and knotted counterparts in *Bf*SOTC and *Xc*AOTC were less accessible to HDX (Fig. 4). Relative to *Bf*SOTC, *Xc*AOTC exhibited significantly more HDX protections within the knotted region, strongly indicating that the higher rigidity within the knotted core region is responsible for the higher unfolding cooperativity and therefore folding stability of *Xc*AOTC with respect to *Bf*SOTC and *Ec*OTC.

In summary, we revealed the potential stabilizing effects of a knotted motif within the OTC family through comparative analyses between the unknotted *Ec*OTC and the knotted *Bf*SOTC and *Xc*AOTC. Our results indicated that the knotted *Xc*AOTC was chemically more stable than *Bf*SOTC and much more so than the unknotted *Ec*OTC. Native HDX-MS analyses supported such findings. HDX-MS affords additional structural information at a resolution of individual peptide fragments regarding the local stabilities of the knotted regions and beyond. While there exists considerable sequence variations among the OTC variants, their overall tertiary and quaternary structures are conserved with the exception of the knotted regions and additional structural motifs in *Ec*OTC (Extra region; Fig. 1) that are distant from the knotted region. The use of HDX-MS effectively helped tease out the folding stabilities of individual structural elements within the three different OTC variants, thus establishing our conclusion that the knotted structural motifs indeed afford enhanced folding stabilities, which are not limited to the local structures but applicable to the global folding stabilities.

Acknowledgement

This work was supported by the Ministry of Science and Technology (105-2113-M-001-005 and 106-2113-M-001-004 for S.-T.D.H., and 106-2811-M-001-111 and 105-2811-M-001-088 for M.K.S.) and Academia Sinica, Taiwan. We thank Dr. Shu-Yu Lin and Mr Ming-Jie Tsai of the Mass Spectrometry Core Facility, at Academia Sinica for assisting the HDX-MS data collection, Dr Meng-Ru Ho of the Biophysics Facility of the Institute of Biological Chemistry, Academia Sinica, and Dr Yun-Tzai Lee and Ms Yen Chen from the Hsu laboratory for assisting data collection. We appreciate the excellent support of the staff of the BL23A beamline at NSRRC for the SEC-SAXS data collections. The manuscript has been proofread and edited by Dr Cindy Lee at the Institute of Biological Chemistry, Academia Sinica, Taiwan.

Appendix A. Supplementary data

Supplementary data related to this article can be found at https://doi.org/10.1016/j.bbrc.2018.06.082.

Transparency document

Transparency document related to this article can be found online at https://doi.org/10.1016/j.bbrc.2018.06.082.

References

[1] J.I. Sulkowska, P. Sulkowski, P. Szymczak, M. Cieplak, Stabilizing effect of knots on proteins, Proc. Natl. Acad. Sci. U.S.A. 105 (2008) 19714–19719.
[2] N.C. Lim, S.E. Jackson, Molecular knots in biology and chemistry, J. Phys. Condens. Matter 27 (2015), 354101.
[3] D.T. Capraro, P.A. Jennings, Untangling the influence of a protein knot on folding, Biophys. J. 110 (2016) 1044–1051.
[4] J.S. Richardson, β-Sheet topology and the relatedness of proteins, Nature 268 (1977) 495–500.
[5] M.L. Mansfield, Are there knots in proteins? Nat. Struct. Biol. 1 (1994) 213–214.
[6] M. Jamroz, W. Niemyska, E.J. Rawdon, A. Stasiak, K.C. Millett, P. Sulkowski, J.I. Sulkowska, KnotProt: a database of proteins with knots and slipknots, Nucleic Acids Res. 43 (2015) D306–D314.
[7] P.F. Faisca, Knotted proteins: a tangled tale of structural biology, Comput. Struct. Biotechnol. J. 13 (2015) 459–468.
[8] T. Christian, R. Sakaguchi, A.P. Perlinska, G. Lahoud, T. Ito, E.A. Taylor, S. Yokoyama, J.I. Sulkowska, Y.M. Hou, Methyl transfer by substrate signaling from a knotted protein fold, Nat. Struct. Mol. Biol. 23 (2016) 941–948.
[9] K. Lim, H. Zhang, A. Tempczyk, W. Krajewski, N. Bonander, J. Toedt, A. Howard, E. Eisenstein, O. Herzberg, Structure of the YibK methyltransferase from *Haemophilus influenzae* (HI0766): a cofactor bound at a site formed by a knot, Proteins 51 (2003) 56–67.
[10] M.K. Sriramoju, Y. Chen, Y.C. Lee, S.-T.D. Hsu, Topologically knotted deubiquitinases exhibit unprecedented mechanostability to withstand the proteolysis by an AAA+ protease, Sci. Rep. 8 (2018) 7076.
[11] A. San Martin, P. Rodriguez-Aliaga, J.A. Molina, A. Martin, C. Bustamante, M. Baez, Knots can impair protein degradation by ATP-dependent proteases, Proc. Natl. Acad. Sci. U.S.A. 114 (2017) 9864–9869.
[12] R. Potestio, C. Micheletti, H. Orland, Knotted vs. unknotted proteins: evidence of knot-promoting loops, PLoS Comput. Biol. 6 (2010) e1000864.
[13] D. Shi, N.M. Allewell, M. Tuchman, From genome to structure and back again:

a family portrait of the transcarbamylases, Int. J. Mol. Sci. 16 (2015) 18836–18864.
[14] R.D. Finn, P. Coggill, R.Y. Eberhardt, S.R. Eddy, J. Mistry, A.L. Mitchell, S.C. Potter, M. Punta, M. Qureshi, A. Sangrador-Vegas, G.A. Salazar, J. Tate, A. Bateman, The Pfam protein families database: towards a more sustainable future, Nucleic Acids Res. 44 (2016) D279–D285.
[15] D. Shi, H. Morizono, X. Yu, L. Roth, L. Caldovic, N.M. Allewell, M.H. Malamy, M. Tuchman, Crystal structure of N-acetylornithine transcarbamylase from *Xanthomonas campestris*: a novel enzyme in a new arginine biosynthetic pathway found in several eubacteria, J. Biol. Chem. 280 (2005) 14366–14369.
[16] D. Shi, H. Morizono, J. Cabrera-Luque, X. Yu, L. Roth, M.H. Malamy, N.M. Allewell, M. Tuchman, Structure and catalytic mechanism of a novel N-succinyl-L-ornithine transcarbamylase in arginine biosynthesis of *Bacteroides fragilis*, J. Biol. Chem. 281 (2006) 20623–20631.
[17] P. Dabrowski-Tumanski, A. Stasiak, J.I. Sulkowska, In search of functional advantages of knots in proteins, PLoS One 11 (2016) e0165986.
[18] Y. Ha, M.T. McCann, M. Tuchman, N.M. Allewell, Substrate-induced conformational change in a trimeric ornithine transcarbamoylase, Proc. Natl. Acad. Sci. U.S.A. 94 (1997) 9550–9555.
[19] D. Shi, X. Yu, L. Roth, H. Morizono, M. Tuchman, N.M. Allewell, Structures of N-acetylornithine transcarbamoylase from *Xanthomonas campestris* complexed with substrates and substrate analogs imply mechanisms for substrate binding and catalysis, Proteins 64 (2006) 532–542.
[20] I. Wang, S.Y. Chen, S.-T.D. Hsu, Unraveling the folding mechanism of the smallest knotted protein, MJ0366, J. Phys. Chem. B 119 (2015) 4359–4370.
[21] I. Wang, S.Y. Chen, S.-T.D. Hsu, Folding analysis of the most complex Stevedore's protein knot, Sci. Rep. 6 (2016) 31514.
[22] L. Jin, B.A. Seaton, J.F. Head, Crystal structure at 2.8 Å resolution of anabolic ornithine transcarbamylase from *Escherichia coli*, Nat. Struct. Biol. 4 (1997) 622–625.
[23] D. Shi, R. Gallegos, J. DePonte 3rd, H. Morizono, X. Yu, N.M. Allewell, M. Malamy, M. Tuchman, Crystal structure of a transcarbamylase-like protein from the anaerobic bacterium *Bacteroides fragilis* at 2.0 Å resolution, J. Mol. Biol. 320 (2002) 899–908.
[24] Y.T.C. Lee, S.-T.D. Hsu, A natively monomeric deubiquitinase UCH-L1 forms highly dynamic but defined metastable oligomeric folding intermediates, J. Phys. Chem. Lett. 9 (2018) 2433–2437.
[25] C. Legrain, V. Stalon, J.P. Noullez, A. Mercenier, J.P. Simon, K. Broman, J.M. Wiame, Structure and function of ornithine carbamoyltransferases, Eur. J. Biochem. 80 (1977) 401–409.
[26] P.J. Snodgrass, The effects of pH on the kinetics of human liver Ornithine–carbamyl phosphate transferase, Biochemistry 7 (1968) 3047–3051.
[27] M.H. Koch, P. Vachette, D.I. Svergun, Small-angle scattering: a view on the properties, structures and structural changes of biological macromolecules in solution, Q. Rev. Biophys. 36 (2003) 147–227.
[28] Y.T.C. Lee, C.Y. Chang, S.Y. Chen, Y.R. Pan, M.R. Ho, S.-T.D. Hsu, Entropic stabilization of a deubiquitinase provides conformational plasticity and slow unfolding kinetics beneficial for functioning on the proteasome, Sci. Rep. 4 (2017) 45174.
[29] L. Konermann, J. Pan, Y.H. Liu, Hydrogen exchange mass spectrometry for studying protein structure and dynamics, Chem. Soc. Rev. 40 (2011) 1224–1234.
[30] S.-T.D. Hsu, A. Bonvin, Atomic insight into the CD4 binding-induced conformational changes in HIV-1 gp120, Proteins: Struct. Funct. Bioinf 55 (2004) 582–593.
[31] N.P. King, A.W. Jacobitz, M.R. Sawaya, L. Goldschmidt, T.O. Yeates, Structure and folding of a designed knotted protein, Proc. Natl. Acad. Sci. U.S.A. 107 (2010) 20732–20737.
[32] L.W. Wang, Y.N. Liu, P.C. Lyu, S.E. Jackson, S.-T.D. Hsu, Comparative analysis of the folding dynamics and kinetics of an engineered knotted protein and its variants derived from HP0242 of *Helicobacter pylori*, J. Phys. Condens. Matter 27 (2015), 354106.